PSFC/JA-12-4

Measurements of hohlraum-produced fast ions.

Zylstra, A.B., Li, C. K., Séguin, F.H., Rosenberg, M.J.,
Rinderknecht, H.G., Sinenian, N., Frenje, J.A., Petrasso, R.D.,
Izumi, N.*, Amendt, P.A.*, Landen, O.L.*, Koch, J.A.*

* Lawrence Livermore National Laboratory

February 2012

Plasma Science and Fusion Center
Massachusetts Institute of Technology
Cambridge MA 02139 USA

This work was supported was supported in part by the U.S. DoE (DE-FG52-09NA29553), LLNL (B580243), LLE (414090-G), the Fusion Science Center at the University of Rochester (415023-G), and the National Laser Users Facility (DE-NA0000877). A. Zylstra is supported by the DoE NNSA Stewardship Science Graduate Fellowship (DE-FC52-08NA28752).

Measurements of hohlraum-produced fast ions

A. B. Zylstra,[a] C. K. Li, F. H. Séguin, M. J. Rosenberg, H. G. Rinderknecht, N. Sinenian, J. A. Frenje, and R. D. Petrasso
Plasma Science and Fusion Center, Massachusetts Institute of Technology, Cambridge, MA 02139, USA
N. Izumi, P. A. Amendt, O. L. Landen, and J. A. Koch
Lawrence Livermore National Laboratory, Livermore, CA 94550, USA

(Dated: 29 February 2012)

We report the first fast ion measurements in indirect-drive experiments, which were taken on OMEGA hohlraum and halfraum shots using simple filtered CR-39, a nuclear track detector, and a charged-particle spectrometer. Protons are observed in two energy regimes that are associated with different fast ion production mechanisms. In the first, resonance absorption at the hohlraum wall early in the laser pulse accelerates runaway electrons. In the second, fast electrons are produced with high energy from the two-plasmon decay (TPD) instability in the exploding laser entrance hole (LEH), or from Stimulated Raman Scattering (SRS) in the underdense gas fill. In both cases, the runaway electrons set up a strong electrostatic field that accelerates the measured ions. The former mechanism is observed to have an energy conversion efficiency $\sim (0.6-4)\times10^{-4}$ into fast protons depending on the hohlraum and drive. The latter mechanism has an estimated conversion efficiency from the main drive of $\sim (0.5-2)\times10^{-5}$ depending on assumptions made.

PACS numbers: 52.38.Kd, 52.70.Nc

I. INTRODUCTION

The goal of Inertial Confinement Fusion (ICF) program is to achieve ignition and energy gain in the laboratory, as first described by Nuckolls et al.[1] A spherical shell of deuterium (D) and tritium (T) is compressed such that the central DT gas becomes hot and dense enough to ignite the fusion reaction $\mathrm{D}+\mathrm{T}\rightarrow{}^4\mathrm{He}+\mathrm{n}$. The central ignition starts a burn wave in the main high-density fuel[2,3]. Currently, the ICF community is focused on upcoming ignition experiments at the National Ignition Facility (NIF)[4].

The National Ignition Campaign (NIC) is using the indirect-drive[5,6] approach to ICF. In indirect-drive, the laser drive is incident on the inner wall of a high-Z cavity (usually cylindrical, and made of Au). This creates a high-temperature ($\sim$ 300 eV for NIF) thermal radiation environment inside the hohlraum. The thermal x-rays then provide the capsule drive: outer layers of the capsule ablator are heated and expand rapidly, driving the remaining ablator and cryogenic fuel inwards. Understanding hohlraum physics is crucial to achieving ignition at the NIF; many fundamental physics questions can be more easily studied at smaller-scale facilities such as OMEGA at the University of Rochester[7].

Fast ions and hot electrons produced in laser-plasma interactions (LPI) are known effects, and studied theoretically[8–11] and experimentally[12,13]. In ICF ignition experiments, hot electrons produced by LPI are energetic enough to penetrate the ablator material and deposit energy in the cryogenic fuel, which increases the fuel adiabat and thus reduces the fuel compressibility. Therefore, understanding hot electron production and preheat is critical for achieving ignition[5].

Additionally, strong electrostatic fields around direct-drive implosions were discovered[14] and studied[15] three decades ago. More recent experiments extensively studied these electric fields[16] and related production of fast ions[17] in direct-drive implosions.

Fast ion production has not been studied in hohlraum experiments, as relevant to the NIC. The NIC design uses gas-filled hohlraums to impede plasma flow at the hohlraum wall[18–20]. This requires a thin window at the laser entrance hole (LEH) to contain the initial gas fill. Since the laser beams overlap at the LEH, this can create complex LPI. Recent experiments measured hot electron production due to LPI at the LEH[21], and attributed the hot electron production to the two-plasmon decay (TPD) instability[22,23].

In this paper, we present the first measurements of fast ions produced in both vacuum and gas-filled hohlraum experiments. Fast ion measurements were conducted with the OMEGA Charged-Particle Spectrometer (CPS) 2, or flat-filtered CR-39. Using three geometries: 2.4mm diameter (scale 1.5) half hohlraums and hohlraums, and 1.2mm diameter (scale 0.75) hohlraums. Experimental configurations were designed and analyzed using VISRAD software[24].

The paper is organized as follows: Sections II and III present the experimental configuration and fast ion data from CPS and flat-filtered CR-39, respectively, Section IV interprets the data, Section V discusses estimates of the conversion efficiency to fast ions on the basis of this data, and finally concluding remarks are made in Section VI.

[a] Electronic mail: zylstra@mit.edu

II. CHARGED-PARTICLE SPECTROMETER RESULTS

A. Experimental Design

1. Scale 1.5 Halfraums

Fig. 1 shows the OMEGA scale 1.5 hohlraum used in these experiments. These hohlraums had a 100% LEH composed of 0.6μm polyimide window. The gas fill was $0.04-0.1\ n_c$ neopentane. The hohlraums are driven from one side only, with 15 beams in 2 cones (Cone 2 at 42° and Cone 3 at 59°), with beams pointed at the LEH center, at a maximum total drive energy of 5.8kJ. The laser drive was a 1ns square pulse (SG1018) using SG4 phase plates and SSD. The hohlraum axis is aligned along the P6-P7 axis in the OMEGA target chamber.

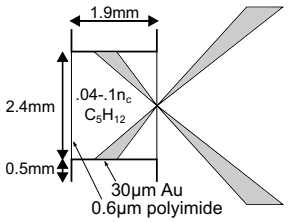

FIG. 1: Cartoon of an OMEGA scale 1.5 halfraum with 100% LEH and gas fill, driven from one side.

The halfraums can be driven from either side. This is shown in Fig. 2. The drive side is hereafter referred to as either P6 or P7, as shown in Fig. 2. The line of sight for CPS 2, which was used for the fast-ion measurement, is also illustrated in the figure.

Drive intensities are calculated for both P6 and P7 drives at the halfraum wall as well as the LEH window, shown in Figs. 3 and 4, shown as viewed from the CPS 2 line of sight. Shown is a full energy halfraum drive, 5.8kJ. Shots were also taken at 1/5 drive energy, in which the calculated intensities should be divided by five. We observe from Figs. 3 and 4 that the peak intensity is $\approx 10^{14}$ W/cm^2 at the halfraum wall, and $\approx 10^{15}$ W/cm^2 at the LEH. In the case where the halfraum is driven from P7 then CPS 2 does not have a clear view of the center of the LEH window.

2. Scale 0.75 Hohlraums

Data was also taken on scale-0.75 hohlraums with a 66% LEH and no gas fill, as shown schematically in Fig. 5. The hohlraums contained a gas-filled capsule. The hohlraum was oriented along the P6-P7 axis as in the other experiments. The hohlraum was driven by 40 beams in cones 1 (21.4°), 2 (42°), and 3 (59°) with a total energy of 20kJ using the main driver without phase plates. The resulting intensity map on the hohlraum wall is shown in Fig. 6, as viewed from the CPS 2 line of sight.

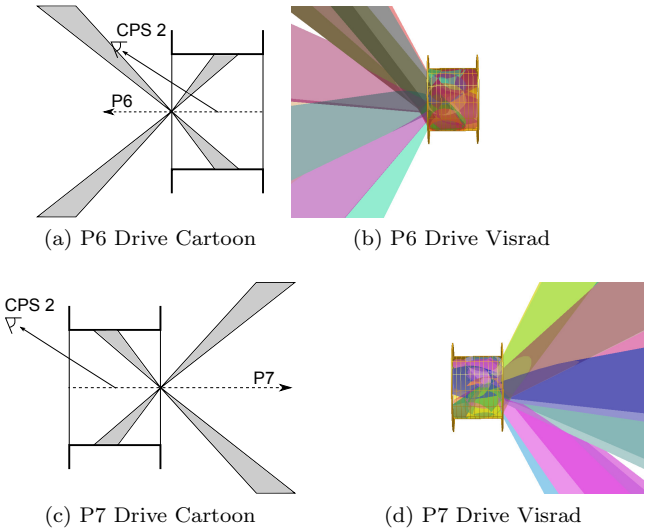

(a) P6 Drive Cartoon (b) P6 Drive Visrad

(c) P7 Drive Cartoon (d) P7 Drive Visrad

FIG. 2: The halfraums can be driven from either side. (a,c) Cartoons of halfraum geometry with P6 or P7 drive, respectively. The CPS 2 line of sight is also shown in these figures. (b,d) Visrad CAD models of halfraum geometry with P6 or P7 drive, respectively.

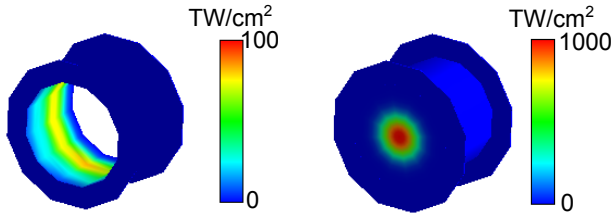

(a) (b)

FIG. 3: P6 drive intensities at the hohlraum wall (a) and at the LEH (b), as viewed from CPS 2.

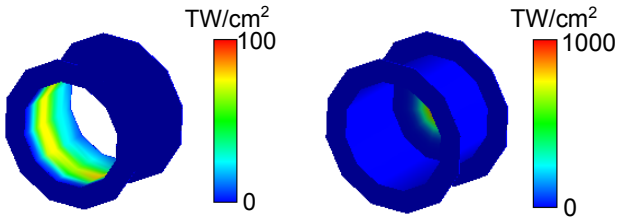

(a) (b)

FIG. 4: P7 drive intensities at the hohlraum wall (a) and at the LEH (b), as viewed from CPS 2.

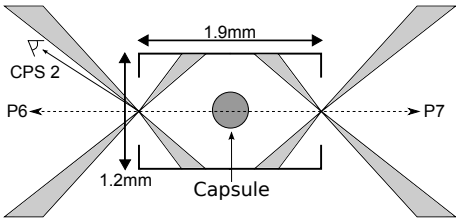

(a)

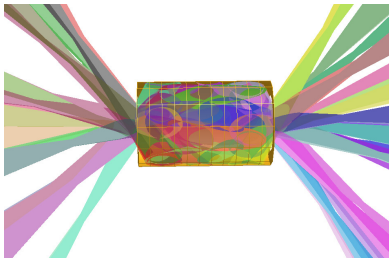

(b)

FIG. 5: (a) Cartoon of an OMEGA scale 0.75 hohlraum with 66% LEH. (b) VISRAD CAD model.

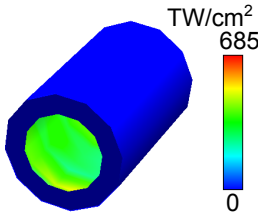

FIG. 6: Drive intensity at the hohlraum wall for the scale 0.75 hohlraum, as viewed from the CPS 2 line of sight.

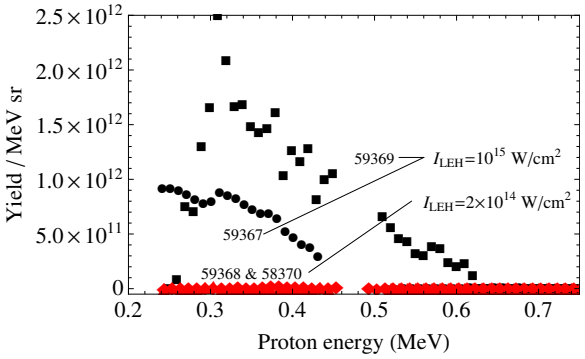

FIG. 7: Charged particle spectra from four OMEGA scale 1.5 gas-filled halfraum shots: 58367 (P7 drive, black circles), 58369 (P6 drive, black squares), 58368 (P7 drive, red triangles), and 58370 (P6 drive, red diamonds). See Table I for experimental configurations.

B. Results

1. Scale 1.5 Halfraums

The CPS-measured charged particle spectra for halfraum shots (as described in Sec. II A 1) are shown in Fig. 7. Data from four OMEGA shots are overplotted. The experimental configuration is summarized in Table I. We can see significant charged-particle production (of order 10^{12} fast protons per MeV per steradian) in two spectra of Fig. 7. These are the higher drive energy (5.8kJ) and thus higher intensity at the hohlraum wall (10^{14} W/cm^2) shots, with the halfraum driven from P7 (Shot 58367) and P6 (Shot 58369). We observe a higher flux of protons and a higher maximum energy for the halfraum driven from P6. This could be because of a preferential acceleration direction due to the plasma waves propagating along the density gradient in the resonance absorption mechanism: In the P6 drive case the diagnostic line of sight is close to the laser propagation angle (Fig. 3), but this is not the case for the P7 drive (Fig. 4).

TABLE I: Experimental configuration for halfraum shots.

Shot	Drive	Energy (kJ)	I_{LEH} (W/cm^2)	I_{Wall} (W/cm^2)
58367	P7	5.8	10^{15}	10^{14}
58368	P7	1.2	2×10^{14}	2×10^{13}
58369	P6	5.8	10^{15}	10^{14}
58370	P6	1.2	2×10^{14}	2×10^{13}

2. Scale 0.75 Hohlraums

The fast ion spectra for two scale 0.75 hohlraum shots, as measured by CPS 2, is shown in Fig. 8. Significant fast ions are observed, at higher fluence per solid angle than the halfraum case in Sec. II B 1 by about an order of magnitude, which is discussed in the following section. Shot 35770 had about 700J more laser energy due to shot-to-shot variations, which explains the higher proton fluence observed.

Fig. 8 also shows a repeatable peak feature at 700-800 keV. In direct-drive implosions, structure in fast ion spectra has been observed[17]. Recent radiography results show charge shells, which are hypothesized as ion acoustic perturbations in the coronal plasma associated with the charged-particle spectral shape[25]. A similar mechanism might be occurring in these hohlraums, which could be investigated with high-resolution charged-particle radiography.

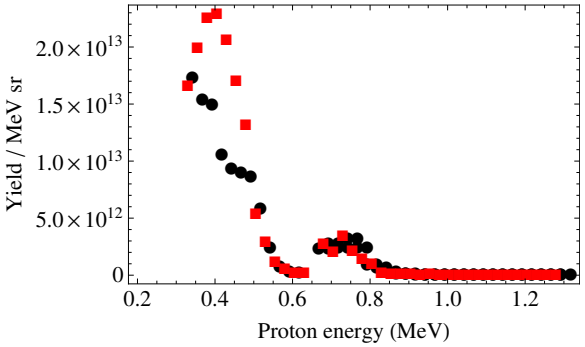

FIG. 8: Charged particle spectra from two OMEGA scale 0.75 vacuum hohlraum shots: 35769 (black circles) and 35770 (red squares). See Section II A 2 for experimental configuration. The laser intensity at the hohlraum wall was 3.5×10^{14}.

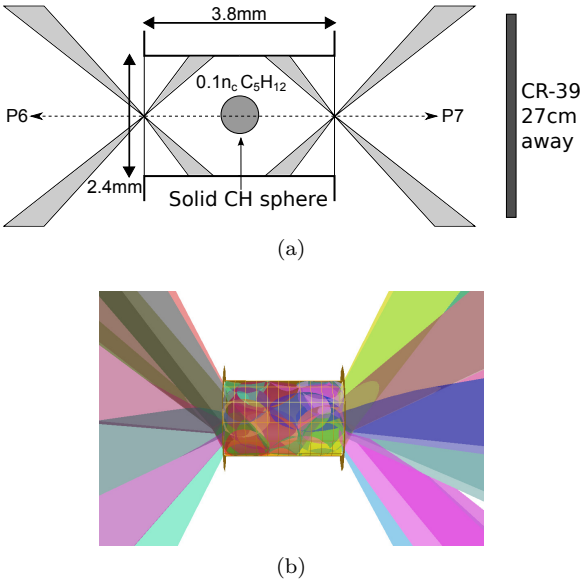

FIG. 9: (a) Cartoon of an OMEGA scale 1.5 hohlraum with 100% LEH and gas fill. (b) VISRAD CAD model of hohlraum geometry with beams.

III. FLAT-FILTERED CR-39 RESULTS

A. Scale 1.5 Hohlraum Design

The 1.5-scale hohlraum is essentially two 1.5-scale halfraums combined, as shown in Fig. 9. The hohlraum is driven from both sides. In this experiment, the full hohlraums had a solid CH capsule in the center, and either a $0.1n_c$ neopentane gas fill or vacuum. The vacuum hohlraums were shot with or without a CH liner on the inner wall. The drive was the same for each side as the equivalent halfraum case, Figs. 3 and 4, to generate the same peak intensities at the wall and LEH. The total drive energy is 11.6kJ.

B. Results

Flat-filtered CR-39 was fielded 27cm away from the target for full gas-filled hohlraum shots, as described in Sec. III A and shown in Fig. 9. The result from this measurement is shown in Fig. 10. The CR-39 is filtered with $\sim 7.5\mu$m of Ta, which gives a minimum detected proton energy of 1.2 MeV. This is at a higher energy than measured in Fig. 7, and the proton fluence for all $E_p > 1.2$MeV is of order 10^{10} protons per steradian. In the center of Fig. 10 we can see a shadow of the capsule in the hohlraum, since it ranges out any protons incident upon it. Protons from the P6-side of the hohlraum (left side of Fig. 9) can be stopped by the capsule since the detector is placed towards P7 (also shown in Fig. 9). The shadow effect shows proton emission towards TCC. Combined with the halfraum data shown in Fig. 7, this further demonstrates that the fast ion emission is in both directions along the hohlraum axis.

In identical radiography experiments using lined and unlined vacuum hohlraums, as recently published[19], the proton fluence on the front piece of flat-filtered CR-39 is of order 10^8 p/sr, which is two orders of magnitude below the fluence observed in Fig. 10. In those previous experiments a fusion proton backlighter was used with $Y \approx 10^9$, which accounts for the proton fluence observed[19]. In these experiments, with identical drive, the two order of magnitude increase in proton fluence on the detector can only be explained by fast protons produced in the hohlraum LEH or gas fill.

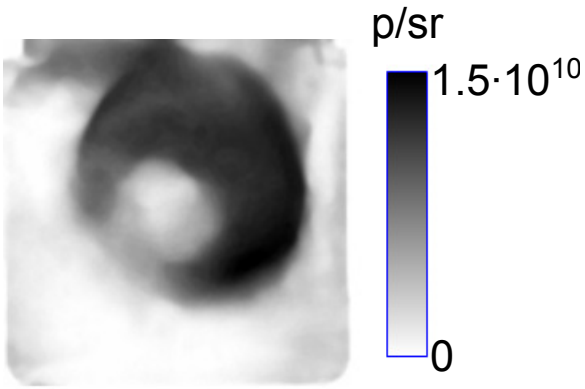

FIG. 10: Flat-filtered CR-39 'radiograph' of a 11.6kJ gas-filled hohlraum implosion with no proton backlighter, plotted as a proton fluence image. The minimum proton energy observable is 1.2 MeV. The CR-39 was placed at 27cm towards P7 (see Fig. 9).

IV. INTERPRETATION

First, we consider the charged particle spectra presented in Sec. II B 2. Since fast protons are observed in the vacuum scale 0.75 hohlraums (Fig. 8) we conclude that these fast protons cannot be produced by any LPI mechanism at the LEH window. This production mechanism is therefore associated with the general hohlraum charging, as discovered using charged-particle radiography[18], which creates $\vec{E}$ fields of order 10^9 V/m. Such strong fields can create runaway ions. The higher yield of fast ions below 1 MeV in the scale 0.75 experiments compared to the scale 1.5 halfraums (Fig. 8 vs 7) is likely due to a $\sim 4\times$ higher total laser energy and intensity at the hohlraum wall in the scale 0.75 experiments (compare Fig. 6 to Figs. 3 and 4).

Since energetic (≥ 1.2 MeV) fast protons are only observed in gas-filled hohlraums we associate this production mechanism with thin plastic LEH window or gas fill.

To explain these observations, we must consider the fundamental LPI instabilities. In general, potentially applicable and well-known LPI mechanisms are: Resonance Absorption (RA), Parametric Decay Instability (PDI), Two-Plasmon Decay (TPD), Stimulated Brillouin Scattering (SBS), and Stimulated Raman Scattering (SRS). For more detail on laser-plasma interaction physics, see Kruer[23].

In general, it is known that fast ion production in laser plasmas is associated with prior hot electron generation, as the runaway hot electrons set up strong $\vec{E}$ fields that accelerate the ions. We therefore focus on mechanisms which can generate hot electrons in this indirect-drive implosion geometry: RA, PDI, TPD, and SRS.

A. Hohlraum mechanisms

An important recent and related result from Li et al.[18] is that large hohlraum fields were observed at the beginning of the laser drive, reaching a strength $|\vec{E}| = 2$ GV/m within the first few hundred ps and monotonically decaying afterwards (see their Fig. 4). Therefore, the hohlraum charging mechanism must generate hot electrons early in time. Since SRS and TPD only occur in underdense plasmas, $\leq n_c/4$ and $n_c/4$, respectively, where n_c is the critical density, these mechanisms would require a large-volume ablated low-density gold plasma. Since previous proton radiography experiments showed that the timescale for hohlraum wall motion[19] is longer than the $\vec{E}$ field generation time[18], SRS and TPD in the ablated wall plasma cannot explain the data.

RA and PDI, which occur at the critical density, are more applicable to the laser-hohlraum wall interaction. RA requires a density gradient from the turning point to the critical density, with a scale length $L = k^{-1}(2\sin^2\alpha)^{-3/2}$, where α is the angle of incidence and k is the wavenumber of a laser photon. Since α is tens of degrees, the term in parentheses is of order unity, and L is of order $1/k$ which is small. Therefore RA will occur early in time when the wall plasma has small gradient lengths. Alternatively, PDI requires a volume of plasma near n_c, which means that it will be more efficient later in time when the gold plasma gradient scales are longer. Since the previously published data[18,19] demonstrate that the hohlraum potential is built up early in time, we associate the hohlraum-charging fast ions with RA.

B. LEH or gas mechanisms

The TPD instability threshold of $(3-5)\times10^{14}$ observed by Regan et al[21] is surpassed at the LEH for full-energy shots, and the entire gas fill is at $n < n_c/4$ so SRS can occur throughout the hohlraum volume for gas-filled experiments. TPD only happens around $n_c/4$. This is applicable to the exploding window plasma where a large amount of material is at (or close to) this density as the window rarefies into vacuum on one side and low-density gas on the other. SRS is applicable to the gas fill, which has the longest scale length of low-density plasma, or the exploded window plasma late in time. While these experiments clearly demonstrate fast proton production at $E_p \geq 1.2$ MeV (Sec. III B and Fig. 10), it is not possible to distinguish between the two potential mechanisms.

V. ESTIMATES OF CONVERSION EFFICIENCY TO PROTONS

A. Hohlraum Resonance Absorption

We can make simple estimates of the conversion efficiency for the 'hohlraum charging' production mechanism due to RA from the spectra shown in Figs. 7 and 8. The total energy in the fast ion population is

$$E = \iint d\Omega dE \, \frac{dY(E,\Omega)}{dE d\Omega} \times E. \tag{1}$$

If we assume that the emission is approximately isotropic far from the target, then

$$E_{\rm hc} = 4\times10^6 \pi e \int_0^\infty \frac{dY(E)}{dE d\Omega} dE \tag{2}$$

where $E_{\rm hc}$ is in J, e is the fundamental charge, and Y is expressed in number per MeV·sr as in Figs. 7 and 8. Here $E_{\rm hc}$ specifically denotes the energy in fast protons due to the hohlraum charging.

Integrating the spectra for the shots shown in Figs. 7 and 8 we calculate the total energy in fast ions and conversion efficiencies ϵ shown in Table II.

TABLE II: Determined conversion efficiencies and total energy carried by fast protons due to the 'hohlraum charging' mechanism.

Shot	Drive (kJ)	$E_{\rm hc}$ (J)	$\epsilon_{\rm hc}$
58367	5.8	0.3	6×10^{-5}
58369	5.8	0.7	1×10^{-4}
35769	20	5.5	3×10^{-4}
35770	20	7.9	4×10^{-4}

B. LEH window TPD or gas-fill SRS

From the data presented in Sec. III we can make order of magnitude estimates of the conversion efficiency for fast ion production due to TPD or SRS when the LEH intensity is about 10^{15} W/cm^2. We assume that the fast ion emission is symmetric around the hohlraum axis and Gaussian with scale θ_0 in the angle from the hohlraum axis. That is, with $\theta = 0$ along the hohlraum axis, the fluence emitted per steradian is

$$F(\theta,\phi) = \frac{Y_p}{4\pi}\frac{\alpha(\theta_0)}{\sqrt{2\pi}\theta_0}e^{-\theta^2/2\theta_0^2}, \qquad (3)$$

where Y_p is the total yield of produced protons and α is a function of θ_0 involving the error function. $\alpha(\theta_0)$ is of order unity.

The simplest case is the hohlraum experiment (Sec. III B), in which case we know F at $\theta \sim 0$ for protons with energies above 1.2 MeV. Setting $F = 1.5\times10^{10}$ protons per steradian and assuming $\theta_0 = 20$ degrees with symmetric emission forwards and backwards from both hohlraum ends we get $Y_p \sim 3\times10^{11}$. As these protons must all be at least 1.2 MeV, the total energy in fast protons with $E_p \geq 1.2$ MeV is $E_{\rm TPD/SRS} \gtrsim 60$mJ. As a fraction of the incident laser energy, the conversion efficiency for this population is $\epsilon_{\rm TPD/SRS} \gtrsim 5\times10^{-6}$. For the short etch times used, an upper bound on proton energies observed is $\sim 3-4$ MeV, implying that $\epsilon_{\rm TPD/SRS} \lesssim 2\times10^{-5}$

We note that from Eq. 3 that for a given fluence at $\theta = 0$ the inferred proton yield scales with $\theta_0/\alpha(\theta_0)$. For $10 \leq \theta_0 \leq 40$, the inferred yield and conversion efficiency will scale by a factor of 4 from the assumption $\theta_0 = 20$ degrees.

VI. CONCLUSIONS

Measurements taken of proton fluence and spectra from OMEGA hohlraum and halfram experiments demonstrate that fast ions are produced in indirect-drive implosions. The data consist of proton spectra from $300-800$ keV, as well as fluence measurements of protons with energy greater than 1.2 MeV.

Observations of fast protons with energies from 300 to 800 keV are observed in both vacuum and gas-filled hohlraums. These protons are associated with the general hohlraum charging seen in charged-particle radiography. We argue that this mechanism is RA, and estimate a conversion efficiency of $\sim (1-4)\times10^{-4}$, depending on the hohlraum and drive. In the flat-filtered CR-39 data significant high-energy (≥ 1.2 MeV) fast protons are observed only for gas-filled hohlraums; we associate this production mechanism with the TPD instability at the exploding window plasma, which is in agreement with observations by Regan et al., or with SRS throughout the underdense gas fill. This mechanism has an estimated conversion efficiency from the main drive of $(0.5-2)\times10^{-5}$ depending on assumptions made.

Future experiments could use several flat-filtered CR-39 detectors to angularly resolve the fast ion emission. The experiment could also be conducted in a geometry that would allow measurements with both magnetic charged particle spectrometers on OMEGA, which could allow a calculation of the emission angle θ_0.

We will also explore advanced radiography measurements of hohlraums using EP-generated protons. This will have the advantage of better spatial and temporal resolution over previous techniques, and could be used to study field structures and mass distributions in the exploding window plasma and plasma bubbles formed on the hohlraum wall. Such measurements would shed light on the fundamental plasma physics behind these observed phenomena.

Previous direct-drive experiments with Au spheres have shown discrepancies in fast proton production[13,17], which could be due to inconsistent hydrogen contaminant levels on the surface, or different plasma scale lengths relative to lower-Z ablators. This could be further investigated on OMEGA.

In addition to fast proton studies, a significant amount of energy can be carried away by heavier ions in direct-drive experiments. The proton measurements imply general ion acceleration, but measuring heavy fast ions produced in indirect-drive experiments would be an important extension of these results.

Simplified experiments to individually measure fast ion production due to indirect-drive relevant mechanisms are motivated by these observations, in particular to determine if SRS in gas filled hohlraums creates an appreciable population of fast ions compared to TPD at the LEH window. Furthermore, this experimental work motivates theoretical and computational study of fast ion production in indirect-drive laser fusion experiments.

ACKNOWLEDGMENTS

The authors thank the engineering and operations staff at the OMEGA facility for their support, as well as J. Schaeffer, R. Frankel, and E. Doeg for contributing to the CR-39 processing.

The work described here was done in part for the first authors's Ph.D. thesis and was supported in part by the U.S. DoE (DE-FG52-09NA29553), LLNL (B580243), LLE (414090-G), the Fusion Science Center at the University of Rochester (415023-G), and the National Laser Users Facility (DE-NA0000877). A. Zylstra is supported by the DoE NNSA Stewardship Science Graduate Fellowship (DE-FC52-08NA28752).

[1] J. Nuckolls, L. Wood, A. Thiessen, and G. Zimmerman, Nature **239**, 139 (1972).
[2] J. Lindl, R. McCrory, E. Campbell, *et al.*, Physics Today **45**, 32 (1992).
[3] S. Atzeni and J. Meyer-ter Vehn, *The physics of inertial fusion* (Clarendon Pr., 2004).
[4] G. Miller, E. Moses, and C. Wuest, Nuclear fusion **44**, S228 (2004).
[5] J. Lindl, Physics of Plasmas **2**, 3933 (1995).
[6] S. Haan, S. Pollaine, J. Lindl, L. Suter, R. Berger, L. Powers, W. Alley, P. Amendt, J. Futterman, W. Levedahl, *et al.*, Physics of Plasmas **2**, 2480 (1995).
[7] T. Boehly, D. Brown, R. Craxton, R. Keck, J. Knauer, J. Kelly, T. Kessler, S. Kumpan, S. Loucks, S. Letzring, *et al.*, Optics communications **133**, 495 (1997).
[8] J. Crow, P. Auer, and J. Allen, Journal of Plasma Physics **14**, 65 (1975).
[9] R. Craxton and M. Haines, Plasma Physics **20**, 487 (1978).
[10] Y. Kishimoto, K. Mima, T. Watanabe, and K. Nishikawa, Physics of Fluids **26**, 2308 (1983).
[11] M. Haines, Physical review letters **78**, 254 (1997).
[12] T. Tan, G. McCall, and A. Williams, Physics of Fluids **27**, 296 (1984).
[13] S. Gitomer, R. Jones, F. Begay, A. Ehler, J. Kephart, and R. Kristal, Physics of Fluids **29**, 2679 (1986).
[14] Y. Gazit, J. Delettrez, T. Bristow, A. Entenberg, and J. Soures, Physical Review Letters **43**, 1943 (1979).
[15] J. Delettrez, A. Entenberg, Y. Gazit, D. Shvarts, J. Virmont, T. Bristow, J. Soures, and A. Bennish, Nuclear fusion **23**, 1135 (1983).
[16] D. Hicks, C. Li, F. Séguin, A. Ram, J. Frenje, R. Petrasso, J. Soures, V. Glebov, D. Meyerhofer, S. Roberts, *et al.*, Physics of Plasmas **7**, 5106 (2000).
[17] D. Hicks, C. Li, F. Séguin, J. Schnittman, A. Ram, J. Frenje, R. Petrasso, J. Soures, D. Meyerhofer, S. Roberts, *et al.*, Physics of Plasmas **8**, 606 (2001).
[18] C. Li, F. Séguin, J. Frenje, R. Petrasso, P. Amendt, R. Town, O. Landen, J. Rygg, R. Betti, J. Knauer, *et al.*, Physical review letters **102**, 205001 (2009).
[19] C. Li, F. Séguin, J. Frenje, M. Rosenberg, R. Petrasso, P. Amendt, J. Koch, O. Landen, H. Park, H. Robey, *et al.*, Science **327**, 1231 (2010).
[20] C. Li, F. Séguin, J. Frenje, M. Rosenberg, A. Zylstra, R. Petrasso, P. Amendt, J. Koch, O. Landen, H. Park, *et al.*, Plasma Physics and Controlled Fusion **52**, 124027 (2010).
[21] S. Regan, N. Meezan, L. Suter, D. Strozzi, W. Kruer, D. Meeker, S. Glenzer, W. Seka, C. Stoeckl, V. Glebov, *et al.*, Physics of Plasmas **17**, 020703 (2010).
[22] A. Simon, R. Short, E. Williams, and T. Dewandre, Physics of Fluids **26**, 3107 (1983).
[23] W. Kruer, *The physics of laser plasma interactions* (Reading, MA (US); Addison-Wesley Publishing Co., 1988).
[24] J. MacFarlane, Journal of Quantitative Spectroscopy and Radiative Transfer **81**, 287 (2003).
[25] F. Séguin, C. Li, M. Manuel, H. Rinderknecht, N. Sinenian, J. Frenje, J. Rygg, D. Hicks, R. Petrasso, J. Delettrez, *et al.*, Physics of Plasmas **19**, 12701 (2012).